

Two-pion exchange three-nucleon potential: $\mathcal{O}(q^4)$ chiral expansion

S. Ishikawa¹ and M. R. Robilotta²

¹*Department of Physics, Science Research Center,
Hosei University, 2-17-1 Fujimi, Chiyoda, Tokyo 102-8160, Japan*

²*Instituto de Física, Universidade de São Paulo,
C.P. 66318, 05315-970, São Paulo, SP, Brazil*

(Dated: November 4, 2018)

Abstract

We present the expansion of the two-pion exchange three-nucleon potential (TPE-3NP) to chiral order q^4 , which corresponds to a subset of all possibilities at this order and is based on the πN amplitude at $\mathcal{O}(q^3)$. Results encompass both numerical corrections to strength coefficients of previous $\mathcal{O}(q^3)$ terms and new structures in the profile functions. The former are typically smaller than 10% whereas the latter arise from either loop functions or non-local gradients acting on the wave function. The influence of the new TPE-3NP over static and scattering three-body observables has been assessed and found to be small, as expected from perturbative corrections.

PACS numbers: 13.75.Cs, 21.30.Fe, 13.75.Gx, 12.39.Fe

I. INTRODUCTION

The research programme for nuclear forces, outlined more than fifty years ago by Taketani, Nakamura, and Sasaki [1], treats pions and nucleons as basic degrees of freedom. This insight proved to be very fruitful. On the one hand, it implies the interconnection of all nuclear processes, both among themselves and with a class of free reactions. On the other, it determines a close relationship between the number of pions involved in a given interaction and its range. As a consequence, the outer components of nuclear forces are dominated by just a few basic subamplitudes, describing either single ($N \rightarrow \pi N$) or multipion ($\pi\pi \rightarrow \pi\pi$, $\pi N \rightarrow \pi N$, $\pi N \rightarrow \pi\pi N$, ...) interactions.

Nevertheless, it took a long time for a theoretical tool to be available which allows the precise treatment of these amplitudes. Nowadays, owing to the development of chiral perturbation theory (ChPT) in association with effective lagrangians [2, 3], the roles of pions and nucleons in nuclear forces can be described consistently. The rationale for this approach is that the quarks u and d , which have small masses, dominate low-energy interactions. One then works with a two-flavor version of QCD and treats their masses as perturbations in a chiral symmetric lagrangian. The systematic inclusion of quark mass contributions is performed by means of chiral perturbation theory, which incorporates low-energy features of QCD into the nuclear force problem. In performing perturbative expansions, one uses a typical scale q , set by either pion four-momenta or nucleon three-momenta, such that $q \ll 1$ GeV.

Nuclear forces are dominated by two-body (NN) interactions and leading contributions are due to the one-pion exchange potential (OPEP), which begins [4] at $\mathcal{O}(q^0)$. The two-pion exchange potential (TPEP) begins at $\mathcal{O}(q^2)$ and, at present, there are two independent expansions up to $\mathcal{O}(q^4)$ in the literature, based on either heavy baryon [5] or covariant [6, 7] ChPT. The TPEP is closely related with the off-shell πN amplitude and, at this order, two-loop diagrams involving intermediate $\pi\pi$ scattering already begin to contribute.

In proper three-nucleon ($3N$) interactions, the leading term is due to the process known as TPE-3NP, in which the pion emitted by a nucleon is scattered before being absorbed by another one. It has been available since long [8–10], involves only tree-level interactions and has the longest possible range. This contribution begins at $\mathcal{O}(q^3)$ and consistency with available NN forces demands the extension of the chiral series for the 3NP up to $\mathcal{O}(q^4)$.

However, the implementation of this programme is not straightforward, since it requires the evaluation of a rather large number of diagrams. With the purpose of exploring the magnitude of $\mathcal{O}(q^4)$ effects, in this work we concentrate on the particular subset of processes which still belong to the TPE-3NP class. Our presentation is divided as follows. In section II we display the general relationship between the TPE-3NP and the πN amplitude, in order to discuss how it affects chiral power counting in the former. The πN amplitude relevant for the $\mathcal{O}(q^4)$ potential is derived in section III and used to construct the three-body interaction in section IV. We concentrate on numerical changes induced into both potential parameters and observables in sections V and VI, whereas conclusions are presented in section VII. There are also four appendices, dealing with kinematics, πN subthreshold coefficients, loop integrals and non-local terms.

II. GENERAL FORMULATION

Potentials to be used into non-relativistic equations can be derived from field theory by means of the T -matrix. In the case of three-nucleon potentials, one starts from the non-relativistic transition matrix describing the process $N(p_1) N(p_2) N(p_3) \rightarrow N(p'_1) N(p'_2) N(p'_3)$, which includes both kernels and their iterations. The former correspond to proper interactions, represented by diagrams which cannot be split into two pieces by cutting positive-energy nucleon lines only, whereas the latter are automatically generated by the dynamical equation. Therefore, just the kernels, denoted collectively by \bar{t}_3 , are included into the potential.

The transformation of a T -matrix into a potential depends on both the dynamical equation adopted and conventions associated with off-shell effects. The latter were discussed in a comprehensive paper by Friar [11]. Here we use the kinematical variables defined in Appendix A and relate \bar{t}_3 to the momentum space potential operator \hat{W} by writing [12]

$$\langle \mathbf{p}'_1, \mathbf{p}'_2, \mathbf{p}'_3 | \hat{W} | \mathbf{p}_1, \mathbf{p}_2, \mathbf{p}_3 \rangle = -(2\pi)^3 \delta^3(\mathbf{P}' - \mathbf{P}) \bar{t}_3(\mathbf{p}'_1, \mathbf{p}'_2, \mathbf{p}'_3, \mathbf{p}_1, \mathbf{p}_2, \mathbf{p}_3). \quad (1)$$

In configuration space, internal dynamics is described by the function

$$W(\mathbf{r}', \boldsymbol{\rho}'; \mathbf{r}, \boldsymbol{\rho}) = - \left[2/\sqrt{3} \right]^6 \int \frac{d\mathbf{Q}_r}{(2\pi)^3} \frac{d\mathbf{Q}_\rho}{(2\pi)^3} \frac{d\mathbf{q}_r}{(2\pi)^3} \frac{d\mathbf{q}_\rho}{(2\pi)^3} \times e^{i[\mathbf{Q}_r \cdot (\mathbf{r}' - \mathbf{r}) + \mathbf{Q}_\rho \cdot (\boldsymbol{\rho}' - \boldsymbol{\rho}) + \mathbf{q}_r \cdot (\mathbf{r}' + \mathbf{r})/2 + \mathbf{q}_\rho \cdot (\boldsymbol{\rho}' + \boldsymbol{\rho})/2]} \bar{t}_3(\mathbf{Q}_r, \mathbf{Q}_\rho, \mathbf{q}_r, \mathbf{q}_\rho), \quad (2)$$

which is to be used in a non-local version of the Schrödinger equation:

$$\left[-\frac{1}{m} \nabla_{\mathbf{r}'}^2 - \frac{1}{m} \nabla_{\boldsymbol{\rho}'}^2 - \epsilon \right] \psi(\mathbf{r}', \boldsymbol{\rho}') = - \left[\sqrt{3}/2 \right]^3 \int d\mathbf{r} d\boldsymbol{\rho} W(\mathbf{r}', \boldsymbol{\rho}'; \mathbf{r}, \boldsymbol{\rho}) \psi(\mathbf{r}, \boldsymbol{\rho}) . \quad (3)$$

Non-local effects are associated with the variables \mathbf{Q}_r and \mathbf{Q}_ρ . When these effects are not too strong, they can be represented by gradients acting on the wave function and the potential W is rewritten as

$$W(\mathbf{r}', \boldsymbol{\rho}'; \mathbf{r}, \boldsymbol{\rho}) = \delta^3(\mathbf{r}' - \mathbf{r}) \delta^3(\boldsymbol{\rho}' - \boldsymbol{\rho}) \left[2/\sqrt{3} \right]^3 V(\mathbf{r}, \boldsymbol{\rho}) . \quad (4)$$

The two-pion exchange three-nucleon potential is represented in Fig. 1a. It is closely related with the πN scattering amplitude, which is $\mathcal{O}(q)$ for free pions and becomes $\mathcal{O}(q^2)$ within the three-nucleon system. As a consequence, the TPE-3NP begins at $\mathcal{O}(q^3)$ and, at this order, it also receives contributions from interactions (c) and (d), which have shorter range. The extension of the chiral series to $\mathcal{O}(q^4)$ requires both the inclusion of single loop effects into processes that already contribute at $\mathcal{O}(q^3)$ and the evaluation of many new amplitudes, especially those associated with diagram (b).

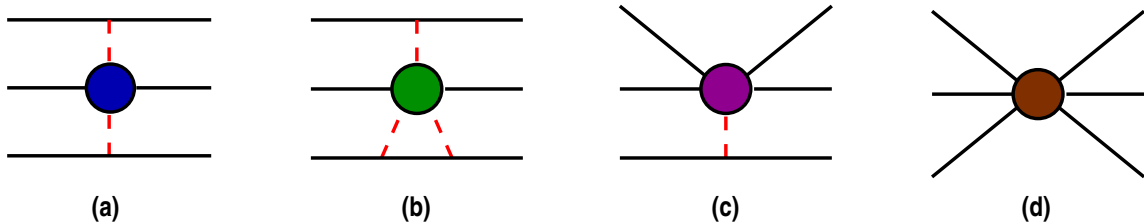


FIG. 1: (Color online) Classes of three-nucleon forces, where full and dashed lines represent nucleons and pions respectively; diagram (a) corresponds to the TPE-3NP.

In this paper we concentrate on the particular set of processes which belong to the TPE-3NP class, represented by the T -matrix $\mathcal{T}_{\pi\pi}$ and evaluated using the kinematical conditions given in Fig. 2. The coupling of a pion to nucleon $i = (1, 2)$ is derived from the usual lowest order pseudo-vector lagrangian $\mathcal{L}^{(1)}$ and the Dirac equation yields the equivalent forms for the vertex

$$(g_A/2f_\pi) [\bar{u} \gamma_5 u]^{(i)} = (mg_A/f_\pi) [\bar{u} \gamma_5 u]^{(i)} , \quad (5)$$

where g_A , f_π and m represent, respectively, the axial nucleon decay, the pion decay and the nucleon mass.

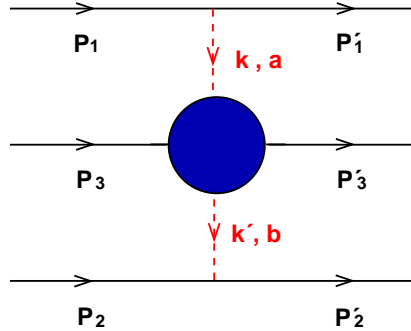


FIG. 2: (Color online) Two-pion exchange three-nucleon potential.

The amplitude for the intermediate process $\pi^a(k)N(p) \rightarrow \pi^b(k')N(p')$ has the isospin structure

$$T_{ba} = \delta_{ab} T^+ + i\epsilon_{bac}\tau_c T^- \quad (6)$$

and Fig. 2 yields

$$\begin{aligned} \mathcal{T}_{\pi\pi} = & - \left[\frac{mg_A}{f_\pi} \right]^2 [\bar{u} \gamma_5 u]^{(1)} [\bar{u} \gamma_5 u]^{(2)} \frac{1}{k^2 - \mu^2} \frac{1}{k'^2 - \mu^2} \\ & [\boldsymbol{\tau}^{(1)} \cdot \boldsymbol{\tau}^{(2)} T^+ - i \boldsymbol{\tau}^{(1)} \times \boldsymbol{\tau}^{(2)} \cdot \boldsymbol{\tau}^{(3)} T^-]^{(3)}, \end{aligned} \quad (7)$$

μ being the pion mass. Results in Appendix A show that $[\bar{u} \gamma_5 u]^{(i)} \rightarrow \mathcal{O}(q)$, whereas pion propagators are $\mathcal{O}(q^{-2})$. As a consequence, in the $\mathcal{O}(q^4)$ expansion of the potential one needs $\mathcal{T}_{\pi\pi}$ to $\mathcal{O}(q)$ and T^\pm to $\mathcal{O}(q^3)$. For on-shell nucleons, the sub amplitudes T^\pm can be written as

$$T^\pm = \bar{u}(\mathbf{p}') \left[D^\pm - \frac{i}{2m} \sigma_{\mu\nu} (p' - p)^\mu K^\nu B^\pm \right] u(\mathbf{p}), \quad (8)$$

with $K = (k' + k)/2$. The dynamical content of the πN interaction is carried by the functions D^\pm and B^\pm and their main properties were reviewed by Höhler [13]. The chiral structure of these sub amplitudes was discussed by Becher and Leutwyler [14, 15] a few years ago, in the framework of covariant perturbation theory, and here we employ their results. As far as power counting is concerned, in Appendix A one finds $[\bar{u}(\mathbf{p}') u(\mathbf{p})]^{(3)} \rightarrow \mathcal{O}(q^0)$ and $[\frac{i}{2m} \bar{u}(\mathbf{p}') \sigma_{\mu\nu} (p' - p)^\mu K^\nu u(\mathbf{p})]^{(3)} \rightarrow \mathcal{O}(q^2)$, indicating that one needs the expansions of D^\pm and B^\pm up to $\mathcal{O}(q^3)$ and $\mathcal{O}(q)$ respectively.

At low and intermediate energies, the πN amplitude is given by a nucleon pole superimposed to a smooth background. One then distinguishes the pseudovector (PV) Born term from a remainder (R) and writes

$$T^\pm = T_{pv}^\pm + T_R^\pm . \quad (9)$$

The former contribution depends on just two observables, namely the nucleon mass m and the πN coupling constant g , as prescribed by the Ward-Takahashi identity [16]. The calculation of these quantities in chiral perturbation theory may involve loops and other coupling constants but, at the end, results must be organized so as to reproduce the physical values of both m and g in T_{pv}^\pm [17]. For this reason, one uses the constant g , instead of (g_A/f_π) , since the former is indeed the observable determined by the residue of the nucleon pole [13, 15, 18]. The pv Born sub amplitudes are given by

$$D_{pv}^+ = \frac{g^2}{2m} \left(\frac{k' \cdot k}{s - m^2} + \frac{k' \cdot k}{u - m^2} \right) , \quad (10)$$

$$B_{pv}^+ = -g^2 \left(\frac{1}{s - m^2} - \frac{1}{u - m^2} \right) , \quad (11)$$

$$D_{pv}^- = \frac{g^2}{2m} \left(\frac{k \cdot k'}{s - m^2} - \frac{k \cdot k'}{u - m^2} - \frac{\nu}{m} \right) , \quad (12)$$

$$B_{pv}^- = -g^2 \left(\frac{1}{s - m^2} + \frac{1}{u - m^2} + \frac{1}{2m^2} \right) , \quad (13)$$

where s and u are the usual πN Mandelstam variables. In the case of free pions, their chiral orders are respectively $[D_{pv}^+, B_{pv}^+, D_{pv}^-, B_{pv}^-] \rightarrow \mathcal{O}[q^2, q^{-1}, q, q^0]$, but important changes do occur when the pions become off-shell.

The amplitudes T_R^\pm receive contributions from both tree interactions and loops. The former can be read directly from the basic lagrangians and correspond to polynomials in $t = (k' - k)^2$ and $\nu = (p' + p) \cdot (k' + k)/4m$, with coefficients given by renormalized LECs [15]. The latter are more complex and depend on Feynman integrals. In the description of πN amplitudes below threshold, one approximates both types of contributions by polynomials and writes [13, 19]

$$X_R = \sum x_{mn} \nu^{2m} t^n , \quad (14)$$

where X_R stands for D_R^+ , B_R^+/ν , D_R^-/ν or B_R^- . The subthreshold coefficients x_{mn} have the status of observables, since they can be obtained by means of dispersion relations applied to scattering data. As such, they constitute an important source of information about the values of the LECs to be used in effective lagrangians.

The isospin odd subthreshold coefficients include leading order terms, which implement the predictions made by Weinberg [20] and Tomozawa [21] for πN scattering lengths, given by

$$D_{WT}^- = \frac{\nu}{2f_\pi^2}, \quad B_{WT}^- = \frac{1}{2f_\pi^2}. \quad (15)$$

For free pions, one has $[D_{WT}^-, B_{WT}^-] \rightarrow \mathcal{O}[q, q^0]$, but these orders of magnitude also change when pions become virtual.

Quite generally, the ranges of nuclear interactions are determined by t -channel exchanges. At $\mathcal{O}(q^3)$, the TPE-3NP involves only single-pion exchanges among different nucleons and has the longest possible range. Another t -channel structure becomes apparent at $\mathcal{O}(q^4)$, associated with the pion cloud of the nucleon, which gives rise to both scalar and vector form factors [18]. These effects extend well beyond 1 fm [22, 23] and a limitation of the power series given by Eq. (14) is that they cannot accommodate these ranges, since Fourier transforms of polynomials yield only δ -functions and its derivatives. In the description of the πN amplitude produced by Becher and Leutwyler [15], one learns that the only sources of medium range (mr) effects are their diagrams k and l , which contain two pions propagating in the t -channel. In our derivation of the TPE-3NP, the loop content of these diagrams is not approximated by power series and, for free pions, the non-pole subamplitudes are written as

$$D_R^+ = D_{mr}^+(t) + [\bar{d}_{00}^+ + d_{10}^+\nu^2 + \bar{d}_{01}^+t]_{(2)} + [d_{20}^+\nu^4 + d_{11}^+\nu^2t + \bar{d}_{02}^+t^2]_{(3)}, \quad (16)$$

$$B_R^+ = B_{mr}^+(t) + [b_{00}^+\nu]_{(1)}, \quad (17)$$

$$D_R^- = D_{mr}^-(t) + [\nu/(2f_\pi^2)]_{(1)} + [\bar{d}_{00}^-\nu + d_{10}^-\nu^3 + \bar{d}_{01}^-t]_{(3)}, \quad (18)$$

$$B_R^- = B_{mr}^-(t) + [1/(2f_\pi^2) + \bar{b}_{00}^-]_{(0)} + [b_{10}^-\nu^2 + \bar{b}_{01}^-t]_{(1)}, \quad (19)$$

where the labels (n) outside the brackets indicate the presence of $\mathcal{O}(q^n)$ leading terms and mr denotes terms associated with the nucleon pion cloud. The *bar* symbol over some coefficients indicates that they do not include both Weinberg-Tomozawa and medium range contributions, which are accounted for explicitly. The functions D_R^\pm and B_R^\pm depend on the parameters f_π , g_A , μ , m and on the LECs c_i and \bar{d}_i , which appear into higher order terms of the effective lagrangian. The subthreshold coefficients are the door through which LECs enter our calculation and their explicit forms are given in Appendix B.

The dynamical content of the $\mathcal{O}(q^3)$ πN amplitude is shown in Fig. 3. The first two diagrams correspond to PV Born amplitudes, whereas the third one represents the Weinberg-

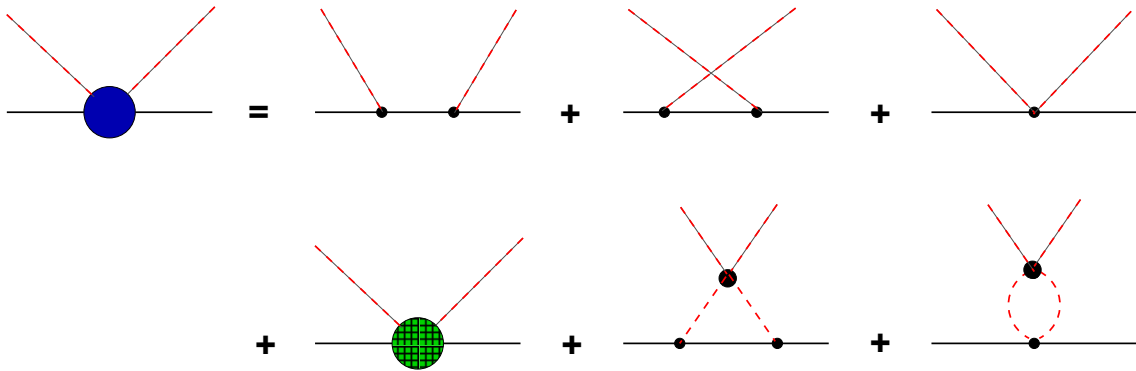


FIG. 3: (Color online) Representation of the πN amplitude used in the construction of the TPE-3NP.

Tomozawa contact interaction, all of them with physical masses and coupling constants. The fourth graph summarizes the terms within square brackets in Eqs. (16-19) and depends on the LECs. Finally, the last two diagrams describe medium range effects owing to the nucleon pion cloud, associated with scalar and vector form factors. This decomposition of the πN amplitude has also been used in our derivation of the two-pion exchange components of the NN interaction [6, 7] and hence the present calculation is consistent with those results.

III. INTERMEDIATE πN AMPLITUDE

The combination of Figs. 2 and 3 gives rise to the TPE-3NP, associated with the six diagrams shown in Fig. 4. In the sequence, we discuss their individual contributions to the subamplitudes D^\pm and B^\pm . We are interested only in the longest possible component of the potential and numerators of expressions are systematically simplified by using $k^2 \rightarrow \mu^2$ and $k'^2 \rightarrow \mu^2$. In configuration space, this corresponds to keeping only those terms which contain two Yukawa functions and neglecting interactions associated with Figs. 1 (c) and 1 (d).

- **diagrams (a) and (b):** The crosses in the nucleon propagators of Figs. 4 (a) and 4 (b) indicate that they do not include forward propagating components, so as to avoid double counting when the potential is used in the dynamical equation. The covariant evaluation of these contributions is based on Eqs. (10-13). Denoting by \bar{p} the momenta of the propagating

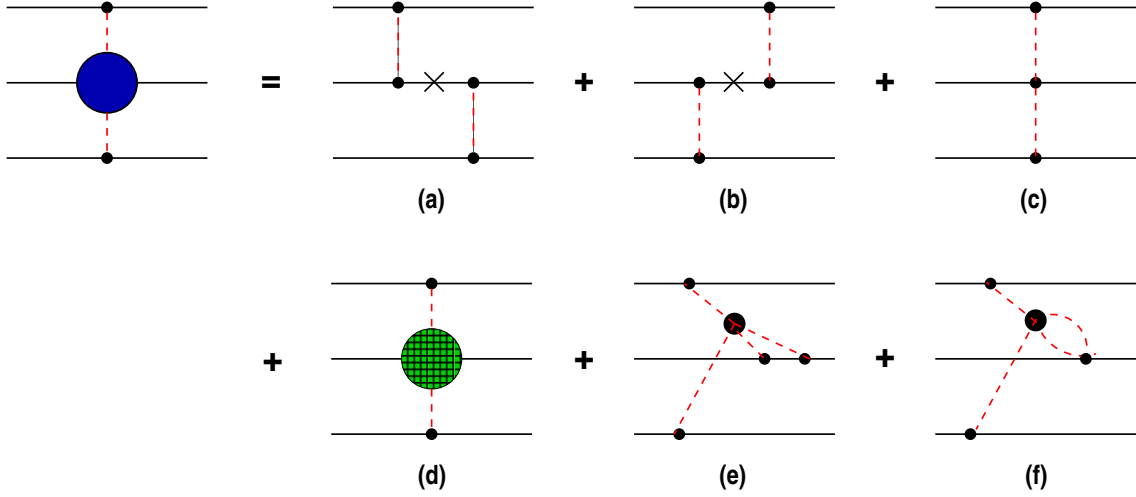


FIG. 4: (Color online) Structure of the $\mathcal{O}(q^4)$ two-pion exchange three-nucleon potential

nucleons, the factors $1/(s-m^2)$ and $1/(u-m^2)$ are decomposed as

$$\frac{1}{(\bar{p}^0)^2 - \bar{E}^2} = \frac{1}{2\bar{E}(\bar{p}^0 - \bar{E})} - \frac{1}{2\bar{E}(\bar{p}^0 + \bar{E})}, \quad (20)$$

with $\bar{E} = \sqrt{m^2 + \bar{\mathbf{p}}^2}$. The first term represents forward propagating nucleons, associated with the iteration of the OPEP, whereas the second one gives rise to connected contributions.

Discarding the former and using the results of Appendix A, one has

$$1/(\{s\} - m^2) \rightarrow -1/\left[4m^2 + \left(3\mathbf{q}_r^2 + \mathbf{q}_\rho^2/3 + 16\mathbf{Q}_\rho^2/3 \pm 10\mathbf{q}_r \cdot \mathbf{Q}_\rho/\sqrt{3} \mp 2\mathbf{q}_\rho \cdot \mathbf{Q}_r/\sqrt{3}\right)\right]. \quad (21)$$

After appropriate truncation, one obtains

$$D_{ab}^+ = -\frac{g^2}{8m^3} (2\mu^2 - t) \rightarrow \mathcal{O}(q^2), \quad (22)$$

$$B_{ab}^+ \rightarrow \mathcal{O}(q^2), \quad (23)$$

$$D_{ab}^- = -\frac{g^2}{2m^2} \nu \rightarrow \mathcal{O}(q^2), \quad (24)$$

$$B_{ab}^- \rightarrow \mathcal{O}(q^2), \quad (25)$$

where we have used the fact that, in the case of virtual pions, $\nu \rightarrow \mathcal{O}(q^2)$.

• **diagrams (c) and (d):** These contributions are purely polynomial, can be read directly

from Eqs. (16-19), and are given by

$$D_{cd}^+ = -\frac{4c_1}{f_\pi^2} \mu^2 + \left[\frac{c_3}{f_\pi^2} + \frac{g_A^4 \mu}{16\pi f_\pi^4} \right] (2\mu^2 - t) \rightarrow \mathcal{O}(q^2), \quad (26)$$

$$B_{cd}^+ \rightarrow \mathcal{O}(q^2), \quad (27)$$

$$D_{cd}^- = \frac{1}{2f_\pi^2} \nu \rightarrow \mathcal{O}(q^2), \quad (28)$$

$$B_{cd}^- = \frac{1}{2f_\pi^2} + \frac{2c_4 m}{f_\pi^2} - \frac{g_A^4 m \mu}{8\pi f_\pi^4} \rightarrow \mathcal{O}(q^0). \quad (29)$$

• **diagrams (e) and (f):** The medium range components of the intermediate πN amplitude are

$$D_e^+ = \frac{g_A^2 \mu}{64\pi^2 f_\pi^4} (2t - \mu^2) [(1 - t/2\mu^2) \Pi_t - 2\pi] \rightarrow \mathcal{O}(q^3), \quad (30)$$

$$D_{ef}^+ \rightarrow \mathcal{O}(q^4), \quad (31)$$

$$B_e^- = \frac{g_A^2 m \mu}{16\pi^2 f_\pi^4} [(1 - t/4\mu^2) \Pi_t - \pi] \rightarrow \mathcal{O}(q), \quad (32)$$

where Π_t is the dimensionless Feynman integral

$$\Pi_t = \int_0^1 da \frac{\mu^2 F(a)}{t - M^2} \quad \leftarrow \quad M = 2\mu/a, \quad F(a) = \frac{8}{a^2} \tan^{-1} \left[\frac{ma \sqrt{1 - a^2}}{\mu(1 - a^2/2)} \right]. \quad (33)$$

The amplitude D_{ef}^- , proportional to ν , is $\mathcal{O}(q^3)$ for free pions and here becomes $\mathcal{O}(q^4)$. Thus, in fact, diagram (f) does not contribute to the TPE-3NP at $\mathcal{O}(q^4)$.

• **full results:** The Golberger-Treiman relation $g/m = g_A/f_\pi$ is valid up to $\mathcal{O}(q^2)$ and can be used in diagrams (a) and (b). One then has

$$D^+ = \frac{\sigma(2\mu^2)}{f_\pi^2} + \frac{(2\mu^2 - t)}{f_\pi^2} \left[-\frac{g_A^2}{8m} + c_3 + \frac{g_A^2(1 + g_A^2)\mu}{16\pi f_\pi^2} - \frac{g_A^2 \mu}{128\pi^2 f_\pi^2} (1 - 2t/\mu^2) \Pi_t \right], \quad (34)$$

where

$$\sigma(t = 2\mu^2) = -4c_1 \mu^2 - \frac{3g_A^2 \mu^3}{32\pi f_\pi^2} \quad (35)$$

is the value of the scalar form factor at the Cheng-Dashen point [14]. The remaining amplitudes read

$$B^+ \rightarrow \mathcal{O}(q^2), \quad (36)$$

$$D^- = \frac{1 - g_A^2}{2f_\pi^2} \nu, \quad (37)$$

$$B^- = \frac{1 + 4c_4 m}{2f_\pi^2} - \frac{g_A^2(1 + 2g_A^2)m\mu}{16\pi f_\pi^4} + \frac{g_A^2 m \mu}{16\pi^2 f_\pi^4} (1 - t/4\mu^2) \Pi_t. \quad (38)$$

The subamplitudes D^\pm and B^\pm begin at $\mathcal{O}(q^2)$ and one needs just the leading terms in the spinor matrix elements of Eq. (8), which is rewritten as

$$T^+ = 2m D^+ , \quad (39)$$

$$T^- = 2m D^- + i \boldsymbol{\sigma}^{(3)} \cdot \mathbf{k}' \times \mathbf{k} B^- , \quad (40)$$

with $D^+ \rightarrow \mathcal{O}(q^2) + \mathcal{O}(q^3)$, $D^- \rightarrow \mathcal{O}(q^2)$, and $B^- \rightarrow \mathcal{O}(q^0) + \mathcal{O}(q)$.

• **$\mathcal{O}(q^3)$ reduction:** In order to compare our amplitudes with previous $\mathcal{O}(q^3)$ results, one notes that, in case corrections are dropped, one would have

$$D^+ = \frac{\sigma(0)}{f_\pi^2} + \frac{(2\mu^2 - t)}{f_\pi^2} \left\{ - \left[\frac{g_A^2}{8m} \right] + c_3 \right\} , \quad (41)$$

$$B^- = \left[\frac{1}{2f_\pi^2} \right] + \frac{2c_4 m}{f_\pi^2} . \quad (42)$$

These expressions agree with those derived directly from a chiral lagrangian [24], except for the terms within square brackets in both D^+ and B^- . The former corresponds to a Born contribution whereas the latter is due to diagram (c) in Fig. 4, associated with the Weinberg-Tomozawa term.

IV. TWO-PION EXCHANGE POTENTIAL

The expansion of the TPE-3NP up to $\mathcal{O}(q^4)$ requires only leading terms in vertices and propagators. In order to derive the non-relativistic potential in momentum space, one divides Eq. (7) by the relativistic normalization factor $\sqrt{2E} \simeq \sqrt{2m}$ for each external nucleon leg and writes¹

$$\begin{aligned} \bar{t}_3 &= \frac{g_A^2}{4f_\pi^2} \frac{1}{\mathbf{k}^2 + \mu^2} \frac{1}{\mathbf{k}'^2 + \mu^2} \boldsymbol{\sigma}^{(1)} \cdot \mathbf{k} \boldsymbol{\sigma}^{(2)} \cdot \mathbf{k}' \\ &\times \left[\boldsymbol{\tau}^{(1)} \cdot \boldsymbol{\tau}^{(2)} D^+ - i \boldsymbol{\tau}^{(1)} \times \boldsymbol{\tau}^{(2)} \cdot \boldsymbol{\tau}^{(3)} \left(D^- + \frac{i}{2m} \boldsymbol{\sigma}^{(3)} \cdot \mathbf{k}' \times \mathbf{k} B^- \right) \right] . \end{aligned} \quad (43)$$

The configuration space potential has the form

$$V_3(\mathbf{r}, \boldsymbol{\rho}) = \boldsymbol{\tau}^{(1)} \cdot \boldsymbol{\tau}^{(2)} V_3^+(\mathbf{r}, \boldsymbol{\rho}) + \boldsymbol{\tau}^{(1)} \times \boldsymbol{\tau}^{(2)} \cdot \boldsymbol{\tau}^{(3)} V_3^-(\mathbf{r}, \boldsymbol{\rho}) + \text{cyclic permutations}, \quad (44)$$

¹ One notes that this expression is identical with Eq. (33) of Ref. [10] divided by $8m^3$.

with

$$\begin{aligned}
V_3^+(\mathbf{r}, \boldsymbol{\rho}) &= C_1^+ \boldsymbol{\sigma}^{(1)} \cdot \hat{\mathbf{x}}_{31} \boldsymbol{\sigma}^{(2)} \cdot \hat{\mathbf{x}}_{23} U_1(x_{31}) U_1(x_{23}) \\
&+ C_2^+ \left\{ (1/9) \boldsymbol{\sigma}^{(1)} \cdot \boldsymbol{\sigma}^{(2)} [U(x_{31}) - U_2(x_{31})] [U(x_{23}) - U_2(x_{23})] \right. \\
&+ (1/3) \boldsymbol{\sigma}^{(1)} \cdot \hat{\mathbf{x}}_{23} \boldsymbol{\sigma}^{(2)} \cdot \hat{\mathbf{x}}_{23} [U(x_{31}) - U_2(x_{31})] U_2(x_{23}) \\
&+ (1/3) \boldsymbol{\sigma}^{(1)} \cdot \hat{\mathbf{x}}_{31} \boldsymbol{\sigma}^{(2)} \cdot \hat{\mathbf{x}}_{31} U_2(x_{31}) [U(x_{23}) - U_2(x_{23})] \\
&+ \left. \boldsymbol{\sigma}^{(1)} \cdot \hat{\mathbf{x}}_{31} \boldsymbol{\sigma}^{(2)} \cdot \hat{\mathbf{x}}_{23} \hat{\mathbf{x}}_{31} \cdot \hat{\mathbf{x}}_{23} U_2(x_{31}) U_2(x_{23}) \right\} \\
&+ C_3^+ \boldsymbol{\sigma}^{(1)} \cdot \nabla_{31}^I \boldsymbol{\sigma}^{(2)} \cdot \nabla_{23}^I \nabla_{31}^I \cdot \nabla_{23}^I [I^0 - 2I^1] , \tag{45}
\end{aligned}$$

$$\begin{aligned}
V_3^-(\mathbf{r}, \boldsymbol{\rho}) &= C_1^- \left\{ (1/9) \boldsymbol{\sigma}^{(1)} \times \boldsymbol{\sigma}^{(2)} \cdot \boldsymbol{\sigma}^{(3)} [U(x_{31}) - U_2(x_{31})] [U(x_{23}) - U_2(x_{23})] \right. \\
&+ (1/3) \boldsymbol{\sigma}^{(3)} \times \boldsymbol{\sigma}^{(1)} \cdot \hat{\mathbf{x}}_{23} \boldsymbol{\sigma}^{(2)} \cdot \hat{\mathbf{x}}_{23} [U(x_{31}) - U_2(x_{31})] U(x_{23}) \\
&+ (1/3) \boldsymbol{\sigma}^{(1)} \cdot \hat{\mathbf{x}}_{31} \boldsymbol{\sigma}^{(2)} \times \boldsymbol{\sigma}^{(3)} \cdot \hat{\mathbf{x}}_{31} U_2(x_{31}) [U(x_{23}) - U_2(x_{23})] \\
&+ \left. \boldsymbol{\sigma}^{(1)} \cdot \hat{\mathbf{x}}_{31} \boldsymbol{\sigma}^{(2)} \cdot \hat{\mathbf{x}}_{23} \boldsymbol{\sigma}^{(3)} \cdot \hat{\mathbf{x}}_{31} \times \hat{\mathbf{x}}_{23} U_2(x_{31}) U_2(x_{23}) \right\} \\
&+ C_2^- \left\{ \boldsymbol{\sigma}^{(1)} \cdot \left(i \nabla_{31}^{wf} - i \nabla_{23}^{wf} \right) \boldsymbol{\sigma}^{(2)} \cdot \hat{\mathbf{x}}_{23} [U(x_{31}) - U_2(x_{31})] U_1(x_{23}) \right. \\
&+ \boldsymbol{\sigma}^{(1)} \cdot \hat{\mathbf{x}}_{31} \boldsymbol{\sigma}^{(2)} \cdot \left(i \nabla_{31}^{wf} - i \nabla_{23}^{wf} \right) U_1(x_{31}) [U(x_{23}) - U_2(x_{23})] \\
&+ \left. 3 \boldsymbol{\sigma}^{(1)} \cdot \hat{\mathbf{x}}_{31} \boldsymbol{\sigma}^{(2)} \cdot \hat{\mathbf{x}}_{23} \left(i \nabla_{31}^{wf} - i \nabla_{23}^{wf} \right) \cdot [\hat{\mathbf{x}}_{31} U_2(x_{31}) U_1(x_{23}) + \hat{\mathbf{x}}_{23} U_1(x_{31}) U_2(x_{23})] \right\} \\
&+ C_3^- \boldsymbol{\sigma}^{(1)} \cdot \nabla_{31}^I \boldsymbol{\sigma}^{(2)} \cdot \nabla_{23}^I \boldsymbol{\sigma}^{(3)} \cdot \nabla_{31}^I \times \nabla_{23}^I [I^0 - I^1/4] . \tag{46}
\end{aligned}$$

The profile functions are written in terms of the dimensionless variables $\mathbf{x}_{ij} = \mu \mathbf{r}_{ij}$ and read

$$U(x) = \frac{e^{-x}}{x} , \tag{47}$$

$$U_1(x) = - \left(1 + \frac{1}{x} \right) \frac{e^{-x}}{x} , \tag{48}$$

$$U_2(x) = \left(1 + \frac{3}{x} + \frac{3}{x^2} \right) \frac{e^{-x}}{x} , \tag{49}$$

$$I^n = - \frac{16\pi}{\mu^2} \int \frac{d\mathbf{k}}{(2\pi)^3} \frac{d\mathbf{k}'}{(2\pi)^3} e^{i(\mathbf{k} \cdot \mathbf{r}_{31} + \mathbf{k}' \cdot \mathbf{r}_{23})} \left[\frac{t}{\mu^2} \right]^n \frac{1}{\mathbf{k}^2 + \mu^2} \frac{1}{\mathbf{k}'^2 + \mu^2} \Pi_t(t) . \tag{50}$$

The last function involves the loop integral given in Eq. (33) and is discussed further in Appendix C. The gradients ∇_{ij}^I act on the functions I^n , whereas the ∇_{ij}^{wf} act *only* on the wave function and give rise to non-local interactions, as discussed in Appendix D.

The strength coefficients are the following combinations of the basic coupling constants

$$C_1^+ = \frac{g_A^2 \mu^4}{64 \pi^2 f_\pi^4} \sigma(2\mu^2), \quad (51)$$

$$C_2^+ = \frac{g_A^2 \mu^6}{32 \pi^2 f_\pi^4 m} \left(-\frac{g_A^2}{8} + m c_3 + \frac{g_A^2 (1 + g_A^2) m \mu}{16 \pi f_\pi^2} \right), \quad (52)$$

$$C_3^+ = \frac{g_A^4 \mu^7}{4096 \pi^3 f_\pi^6}, \quad (53)$$

$$C_1^- = \frac{g_A^2 \mu^6}{256 \pi^2 f_\pi^4 m} \left(1 + 4m c_4 - \frac{g_A^2 (1 + 2g_A^2) m \mu}{8 \pi f_\pi^2} \right), \quad (54)$$

$$C_2^- = \frac{g_A^2 (g_A^2 - 1) \mu^6}{768 \pi^2 f_\pi^4 m}, \quad (55)$$

$$C_3^- = -\frac{g_A^4 \mu^7}{2048 \pi^3 f_\pi^6}. \quad (56)$$

V. STRENGTH COEFFICIENTS

The strength constants of the potential involve a blend of four well determined parameters, namely $m = 938.28$ MeV, $\mu = 139.57$ MeV, $g_A = 1.267$ and $f_\pi = 92.4$ MeV, with the scalar form factor at the Cheng-Dashen point and the LECs c_3 and c_4 , which are less precise. As far as $\sigma(2\mu^2)$ is concerned, we rely on the results [25] $\sigma(2\mu^2) - \sigma(0) = 15.2 \pm 0.4$ MeV, $\sigma(0) = 45 \pm 8$ MeV, and adopt the central value $\sigma(2\mu^2) = 60$ MeV. The values quoted for the LECs in the literature vary considerably, depending on the empirical input employed and the chiral order one is working at. A sample of values is given in Table I.

Our work is based on the $\mathcal{O}(q^3)$ expansion of the intermediate πN amplitude and, for the sake of consistency, one must use LECs extracted at the same order. The kinematical conditions of the three-body interaction are such that the variable ν is $\mathcal{O}(q^2)$, an order of magnitude smaller than the threshold value, $\nu = \mu$. This makes information encompassed in the subthreshold coefficients better suited to this problem and we use results from Appendix

TABLE I: Some values of the LECs c_3 and c_4 ; m is the nucleon mass.

Reference	Chiral order	πN input	$m c_3$	$m c_4$
[26]	3	amplitude at $\nu = 0, t = 0$	-5.00 ± 1.43	3.62 ± 0.04
[26]	3	amplitude at $\nu = 0, t = 2\mu^2/3$	-5.01 ± 1.01	3.62 ± 0.04
[27]	3	scattering amplitude	-5.69 ± 0.04	3.03 ± 0.16
[15]	4	subthreshold coefficients	-3.4	2.0
[15]	4	scattering lengths	-4.2	2.3
tree	2	subthreshold coefficients	-3.6	2.0
this work	3	subthreshold coefficients	-4.9	3.3

B in order to write

$$m c_3 = -m f_\pi^2 d_{01}^+ - \frac{g_A^4 m \mu}{16 \pi f_\pi^2} - \frac{77 g_A^2 m \mu}{768 \pi f_\pi^2}, \quad (57)$$

$$m c_4 = \frac{f_\pi^2 b_{00}^-}{2} - \frac{1}{4} + \frac{g_A^2 (1 + g_A^2) m \mu}{16 \pi f_\pi^2}. \quad (58)$$

Adopting the values for the subthreshold coefficients given by Höhler [13], namely $d_{01}^+ = 1.14 \pm 0.02 \mu^{-3}$ and $b_{00}^- = 10.36 \pm 0.10 \mu^{-2}$, one finds the figures shown in the last row of Table I. These, in turn, produce the strength coefficients displayed in Table II. For the sake of comparison, we also quote values employed in our earlier calculation [10] and in two TM' versions [28] of the Tucson-Melbourne potential [8].

TABLE II: Strength coefficients in MeV.

reference	C_1^+	C_2^+	C_3^+	C_1^-	C_2^-	C_3^-
this work	0.794	-2.118	0.034	0.691	0.014	-0.067
Brazil [10]	0.92	-1.99	-	0.67	-	-
TM'(93) [28]	0.60	-2.05	-	0.58	-	-
TM'(99) [28]	0.91	-2.26	-	0.61	-	-

Changes in these parameters represent theoretical progress achieved over more than two decades and it is worth investigating their origins in some detail. With this purpose in mind, we compare present results with those of our previous $\mathcal{O}(q^3)$ calculation [10]. At the

chiral order one is working here, new qualitative effects begin to show up, associated with both loops and non-local interactions. They are represented by terms proportional to the coefficients C_3^+ , C_2^- and C_3^- in Eqs. (45) and (46).

The πN coupling is now described by $g_A^2 \mu^2 / f_\pi^2 = 3.66$ whereas, previously, the factor $g^2 \mu^2 / m^2 = 3.97$ was used. From a conceptual point of view, the latter should be preferred, since g is indeed the proper coupling observable. In chiral perturbation theory, the difference between both forms is ascribed to the parameter $\Delta_{GT} = -2d_{18}\mu^2/g$, which describes the Goldberger-Treiman discrepancy [15]. As this is a $\mathcal{O}(q^2)$ effect, both forms of the coupling become equivalent in the present calculation. On the other hand, the empirical value of g is subject to larger uncertainties and the form based on g_A is more precise. Our present choice accounts for a decrease of 8% in all parameters.

The relations $C_1^+ \leftrightarrow C_s$, $C_2^+ \leftrightarrow C_p$ and $C_1^- \leftrightarrow -C'_p$ allow one to compare Eqs. (45) and (46) with Eq. (67) of Ref. [10]. One notes that the latter contains an unfortunate misprint in the sign of the term proportional to C'_p , as pointed out in Ref. [29]. In the earlier calculation, the coefficient C_s was based on a parameter [30] $\alpha_\sigma = 1.05\mu^{-1}$, which corresponds to $\sigma(2\mu^2) = 64$ MeV. The results of Table II show that the values of C_2^+ and C_1^- are rather close to those of C_p and $-C'_p$. This can be understood by rewriting Eqs. (52) and (54) in terms of the subthreshold coefficient d_{01}^+ and b_{00}^- as follows

$$C_2^+ = -\frac{g_A^2 \mu^6}{32 \pi^2 f_\pi^4 m} \left(m f_\pi^2 d_{01}^+ + \frac{g_A^2}{8} + \left[\frac{29g_A^2 m \mu}{768\pi f_\pi^2} \right] \right), \quad (59)$$

$$C_1^- = \frac{g_A^2 \mu^6}{128 \pi^2 f_\pi^4 m} \left(f_\pi^2 b_{00}^- + \left[\frac{g_A^2 m \mu}{16\pi f_\pi^2} \right] \right). \quad (60)$$

Numerically, this amounts to $C_2^+ = -(1.845 + 0.110 + [0.163])$ MeV and $C_1^- = (0.624 + [0.067])$ MeV. The second term in the former equation was overlooked in Ref. [10] and should have been considered there. The square brackets² correspond to next-to-leading order contributions and yield corrections of about 8% and 11% to the leading terms in C_2^+ and C_1^- , respectively.³ As the model used in Ref. [10] was explicitly designed to reproduce the subthreshold coefficients quoted by Höhler [13], it produces the very same contributions as the first terms in Eqs. (59) and (60).

² These factors can be traced back to loop diagrams in Fig. 3 and are dynamically related with the term proportional to C_3^\pm , as we discuss in Appendix C.

³ When comparing the new coefficients with those in the second row of Table II, one should also take into account the 8% effect due to the Goldberger-Treiman discrepancy.

VI. NUMERICAL RESULTS FOR THREE-NUCLEON SYSTEMS

In order to test the effects of the TPE-3NP at $\mathcal{O}(q^4)$, in this section, we present some numerical results of Faddeev calculations for three-nucleon bound and scattering states. The calculations are based on a configuration space approach, in which we solve the Faddeev integral equations [31–33],

$$\begin{aligned} \Phi_3 = & \Xi_{12,3} + \frac{1}{E + i\epsilon - H_0 - V_{12}} \\ & \times [V_{12}(\Phi_1 + \Phi_2) + W_3(\Phi_1 + \Phi_2 + \Phi_3)], \\ & \text{(and cyclic permutations),} \end{aligned} \quad (61)$$

where $\Xi_{12,3}$, which does not appear in the bound state problem, is an initial state wave function for the scattering problem, H_0 is a three-body kinetic operator in the center of mass, V_{12} is a nucleon-nucleon (2NP) potential between nucleons 1 and 2, and W_3 is the 3NP displayed in Fig. 2. Partial wave states of a 3N system, in which both NN and 3N forces act, are restricted to those with total NN angular momenta $j \leq 6$ for bound state calculations, and $j \leq 3$ for scattering state calculations. The total 3N angular momentum (J) is truncated at $J = 19/2$, while 3NP is switched off for 3N states with $J > 9/2$ for scattering calculations. These truncation procedures are confirmed to give converged results for the purposes of the present work.

When just local terms are retained, \bar{t}_3 in Eq. (43) can be cast in the conventional form [8–10]

$$\begin{aligned} \bar{t}_3 = & -\frac{g_A^2}{4f_\pi^2} \frac{F(\mathbf{k}^2)}{\mathbf{k}^2 + \mu^2} \frac{F(\mathbf{k}'^2)}{\mathbf{k}'^2 + \mu^2} (\boldsymbol{\sigma}^{(1)} \cdot \mathbf{k})(\boldsymbol{\sigma}^{(2)} \cdot \mathbf{k}') \\ & \times \left[(\boldsymbol{\tau}^{(1)} \cdot \boldsymbol{\tau}^{(2)}) \{a + b(\mathbf{k} \cdot \mathbf{k}')\} \right. \\ & \left. - (i\boldsymbol{\tau}^{(1)} \times \boldsymbol{\tau}^{(2)} \cdot \boldsymbol{\tau}^{(3)})(i\boldsymbol{\sigma}^{(3)} \cdot \mathbf{k}' \times \mathbf{k})d \right], \end{aligned} \quad (62)$$

where the coefficients, a , b , and d are related with our potential strength coefficients by

$$[C_1^+, C_2^+, C_1^-] = \frac{1}{(4\pi)^2} \left(\frac{g_A}{2f_\pi} \right)^2 [-a\mu^4, b\mu^6, -d\mu^6]. \quad (63)$$

The values of the coefficients, a , b , and d for the TPE-3NP at $\mathcal{O}(q^4)$ are shown in Table III, as BR- $\mathcal{O}(q^4)$. In this table, the values for the older version of the Brazil TPE-3NP, BR(83) [10], and the potential up to $\mathcal{O}(q^3)$ given by Eqs. (41-42), BR- $\mathcal{O}(q^3)$, are shown as well.

TABLE III: Coefficients a , b , and d of the TPE-3NP.

3NP	$a \mu$	$b \mu^3$	$d \mu^3$
BR- $\mathcal{O}(q^4)$	-0.981	-2.617	-0.854
BR- $\mathcal{O}(q^3)$	-0.736	-3.483	-1.204
BR(83)	-1.05	-2.29	-0.768

In Eq. (62), the function $F(\mathbf{k}^2)$ represents a π NN form factor. We apply a dipole form factor with the cut off mass Λ , $\left(\frac{\Lambda^2 - \mu^2}{\Lambda^2 + \mathbf{k}^2}\right)^2$, which modifies the profile functions $U(x)$, $U_1(x)$, and $U_2(x)$ in Eqs. (47-49) as

$$U(x) = \frac{e^{-x}}{x} - \frac{e^{-\bar{\Lambda}x}}{x} \left(1 + \frac{\bar{\Lambda}^2 - 1}{2\bar{\Lambda}}x\right), \quad (64)$$

$$U_1(x) = -\left(1 + \frac{1}{x}\right) \frac{e^{-x}}{x} + \bar{\Lambda}^2 \left(1 + \frac{1}{\bar{\Lambda}x}\right) \frac{e^{-\bar{\Lambda}x}}{\bar{\Lambda}x} + \left(\frac{\bar{\Lambda}^2 - 1}{2}\right) e^{-\bar{\Lambda}x}, \quad (65)$$

$$U_2(r) = \left(1 + \frac{3}{x} + \frac{3}{x^2}\right) \frac{e^{-x}}{x} - \bar{\Lambda}^3 \left(1 + \frac{3}{\bar{\Lambda}x} + \frac{3}{(\bar{\Lambda}x)^2}\right) \frac{e^{-\bar{\Lambda}x}}{\bar{\Lambda}x} - \frac{\bar{\Lambda}(\bar{\Lambda}^2 - 1)}{2} \left(1 + \frac{1}{\bar{\Lambda}x}\right) e^{-\bar{\Lambda}x}, \quad (66)$$

with $\bar{\Lambda} = \Lambda/\mu$.

We choose the Argonne V_{18} model (AV18) [34] for a realistic NN potential, by which the triton binding energy (B_3) becomes 7.626 MeV, underbinding it by about 0.9 MeV compared to the empirical value, 8.482 MeV. As it is well known, the introduction of the TPE-3NP remedies this deficiency. The amount of attractive contribution depends on the cutoff mass Λ , as shown in Fig. 5. The solid curve shows the dependence of B_3 on Λ for the calculation with the BR- $\mathcal{O}(q^4)$ 3NP in addition to the AV18 2NP (AV18+BR- $\mathcal{O}(q^4)$). In the figure, the empirical value and the AV18 result are displayed by the dashed and dotted horizontal lines, respectively. Due to the strong attractive character of the 3NP, B_3 is reproduced by choosing a rather small value of Λ , namely 660 MeV. In the same figure, the Λ -dependence of B_3 for AV18+BR- $\mathcal{O}(q^3)$ is displayed by a dashed curve and that for the AV18+BR(83) by a dotted curve. From these curves we see that AV18+BR- $\mathcal{O}(q^3)$ reproduces B_3 for $\Lambda = 620$ MeV and AV18+BR(83) for $\Lambda = 680$ MeV. In other words, the BR- $\mathcal{O}(q^4)$ 3NP is slightly

more attractive than the BR(83) 3NP and a large attractive effect occurs when one moves from the TPE $\mathcal{O}(q^4)$ 3NP to the $\mathcal{O}(q^3)$ 3NP. This tendency is strongly correlated with the magnitude of the coefficient b , as shown in Table III. This can be understood as a dominant contribution to B_3 from the component of the TPE-3NP associated with the coefficients b . This dominance is shown in Table IV, where we tabulate calculated B_3 for the AV18 plus the BR- $\mathcal{O}(q^4)$ 3NP and plus each term of the BR- $\mathcal{O}(q^4)$ coming from the coefficients a , b , and d .

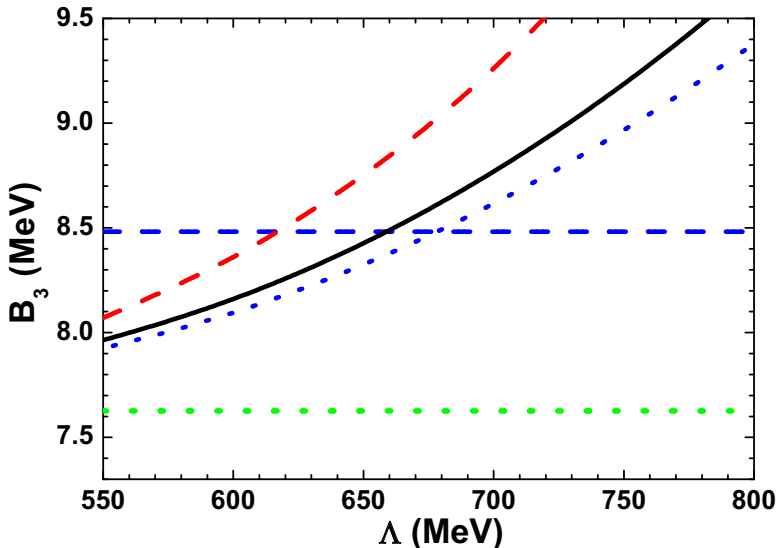


FIG. 5: (Color online) The triton binding energy B_3 as functions of the cutoff mass Λ of the πNN dipole form factor. The solid curve denotes the result for AV18+BR- $\mathcal{O}(q^4)$, the dashed curve for AV18+BR- $\mathcal{O}(q^3)$, and the dotted curve for AV18+BR(83). The horizontal lines denote the AV18 result (dotted line) and the empirical value (dashed line).

In Fig. 6, we compare six calculated observables for proton-deuteron elastic scattering, namely differential cross sections $\sigma(\theta)$, vector analyzing powers of the proton $A_y(\theta)$ and of the deuteron $iT_{11}(\theta)$, and tensor analyzing powers of the deuteron $T_{20}(\theta)$, $T_{21}(\theta)$, and $T_{22}(\theta)$, at incident proton energy $E_N^{lab} = 3.0$ MeV, (or incident deuteron energy $E_d^{lab} = 6.0$ MeV,) with experimental data of Ref. [35, 36]. In the figure, the solid curves designate the AV18 calculations and the dashed curves the AV18+BR- $\mathcal{O}(q^4)$ calculations, which are almost indistinguishable from the AV18+BR- $\mathcal{O}(q^3)$ and AV18+BR(83) calculations, once

TABLE IV: Triton binding energy for the AV18 2NP plus the BR- $\mathcal{O}(q^4)$ 3NP for each term of the BR- $\mathcal{O}(q^4)$ 3NP with $\Lambda = 660$ MeV. ΔB_3 means the difference of the calculated binding energy from that of the AV18 calculation.

	B_3 (MeV)	ΔB_3 (MeV)
AV18+BR- $\mathcal{O}(q^4)$	8.492	0.866
AV18+BR- $\mathcal{O}(q^4)$ -a	7.673	0.047
AV18+BR- $\mathcal{O}(q^4)$ -b	8.241	0.615
AV18+BR- $\mathcal{O}(q^4)$ -d	7.787	0.161

the cut off masses are chosen so that B_3 is reproduced.

It is reminded that the TPE-3NF gives minor effects on the vector analyzing powers. This happens because the exchange of pions gives essentially scalar and tensor components of nuclear interaction in spin space, which are not so effective to the vector analyzing powers. On the other hand, as is noticed in Refs. [37, 38], at $E_N^{lab} = 3.0$ MeV, the TPE-3NP gives a wrong contribution to the tensor analyzing power $T_{21}(\theta)$ around $\theta = 90^\circ$.

In Fig. 7, we compare calculations of observables in neutron-deuteron elastic scattering at $E_N^{lab} = 28.0$ MeV with experimental data of proton-deuteron scattering Ref. [39]. At this energy, discrepancies between the calculations and the experimental data in the vector analyzing power $iT_{11}(\theta)$ appear at $\theta \sim 100^\circ$, where $iT_{11}(\theta)$ has a minimum, and at $\theta \sim 140^\circ$, where $iT_{11}(\theta)$ has a maximum, which are not compensated by the introduction of the TPE-3NP. On the other hand, while the AV18 calculation almost reproduces the experimental data of $T_{21}(\theta)$ at $\theta \sim 90^\circ$, the introduction of the TPE-3NP gives a wrong effect, as in the $E_N^{lab} = 3$ MeV case.

These results set the stage for the introduction of terms associated with the coefficients C_3^+ , C_2^- , and C_3^- , Eqs. (44-45), which are new features of the $\mathcal{O}(q^4)$ expansion of the TPE-3NP. Terms proportional to C_3^\pm , which include the rather complicated function $I(\mathbf{r}_{31}, \mathbf{r}_{23})$ given in Appendix C, arise from a loop integral, Eq. (33). On the other hand, the term with C_2^- corresponds to a non-local potential and includes the gradient operator ∇_{ij}^{wf} , which acts on the wave function and arises from the kinematical variable ν . Both kinds of contributions are not expressed in the conventional local form shown in Eq. (62), which involves only the coefficients C_1^+ , C_2^+ , and C_1^- , and the full evaluation of their effects would require an

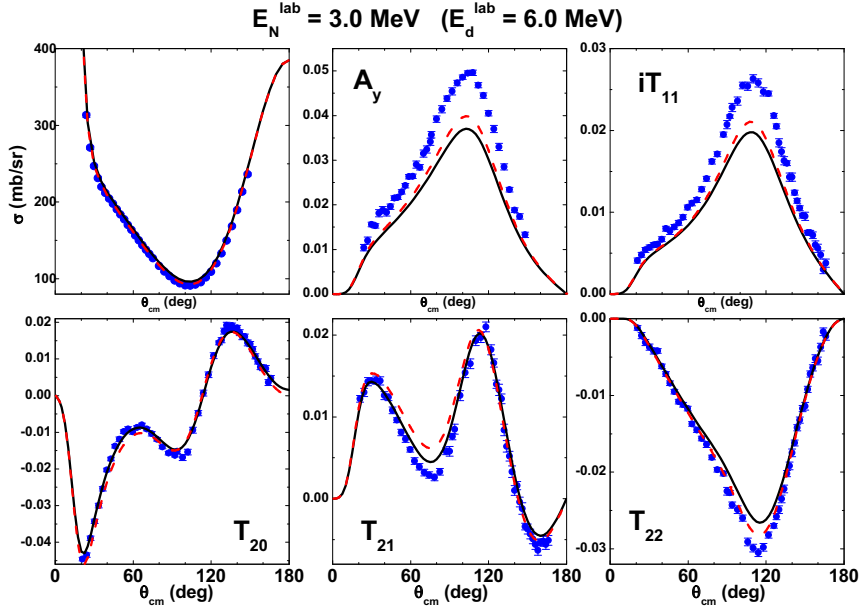


FIG. 6: (Color online) Proton-deuteron elastic scattering observables at $E_N^{\text{lab}} = 3.0$ MeV. Solid curves are calculations for the AV18 potential, and dashed curves for the AV18+BR- $\mathcal{O}(q^4)$. Experimental data are taken from Refs. [35, 36].

extensive rebuilding of large numerical codes. However, the coefficients of the new terms are small, and in this exploratory paper we estimate their influence over observables as follows.

The function $I(\mathbf{r}_{31}, \mathbf{r}_{23})$ is approximated by Eq. (C11), which amounts to replacing $\Pi_t(t)$ by a factor $-\pi$. Further, the kinematical factors in front of $\Pi_t(t)$ in Eqs. (34) and (38), namely $1 - 2t/\mu^2$ and $1 - t/4\mu^2$, are approximately evaluated by putting $t \approx 2\mu^2$, which yields -3 and $1/2$, respectively. By this procedure, the coefficients C_3^+ and C_3^- are absorbed into C_2^+ and C_1^- , or in b and d respectively, and one has

$$\Delta C_2^+ = -3C_3^+, \quad \Delta C_1^- = C_3^-/2. \quad (67)$$

Numerically, this corresponds to $\Delta C_2^+ = -0.102$ MeV $\sim \frac{1}{20}C_2^+$ and $\Delta C_1^- = -0.034$ MeV $\sim -\frac{1}{20}C_1^-$, or $\Delta b = -0.125(\mu^{-3})$ and $\Delta d = 0.042(\mu^{-3})$. The net change produced in the triton binding energy is $+0.026$ MeV ($+0.037$ MeV from ΔC_2^+ and -0.011 MeV from ΔC_1^-), just about $1/30$ of the total increase in B_3 due to the local terms of the BR- $\mathcal{O}(q^4)$ TPE-3NP.

The non-local term proportional to C_2^- is more involved and we restrict ourselves to a rough assessment of its role. We replace the variable ν by a constant $\langle \nu \rangle$ and assume, for

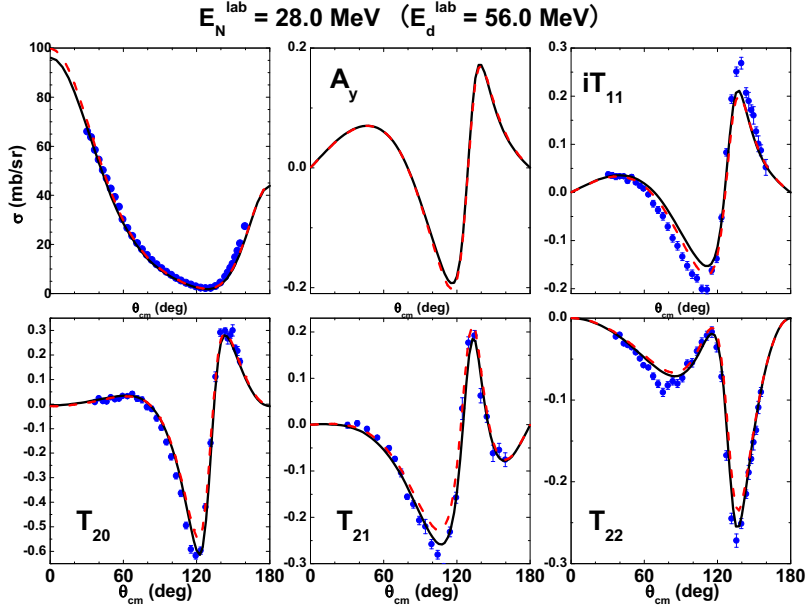


FIG. 7: (Color online) Nucleon-deuteron elastic scattering observables at $E_N^{\text{lab}} = 28.0$ MeV. Curves are calculations for neutron-deuteron scattering. Solid curves denote calculations for the AV18 potential and dashed curves for the AV18+BR- $\mathcal{O}(q^4)$. Experimental data are those for proton-deuteron scattering taken from Ref. [39].

example, that $\langle \nu \rangle = \frac{\mu^2}{4m}$. This changes the C_2^- term in Eq. (46) into the very simple form

$$V_3^-(\mathbf{r}, \boldsymbol{\rho}) = C_1^-(\dots) + i\tilde{C}_2^-\boldsymbol{\sigma}^{(1)} \cdot \hat{\mathbf{x}}_{31}\boldsymbol{\sigma}^{(2)} \cdot \hat{\mathbf{x}}_{23}U_1(x_{31})U_1(x_{23}) + C_3^-(\dots), \quad (68)$$

with

$$\tilde{C}_2^- = -\frac{g_A^2}{4f_\pi^2} \frac{1 - g_A^2}{2f_\pi^2} \langle \nu \rangle \frac{\mu^4}{(4\pi)^2} = -\frac{g_A^2(1 - g_A^2)\mu^6}{512\pi^2 f_\pi^4 m} = 0.021 \text{ MeV}. \quad (69)$$

Except for the isospin factor, this term is similar to that with C_1^+ (or a), which adds about 0.05 MeV to the triton binding energy. Since the potential strength \tilde{C}_2^- is about 3 % of C_1^+ , its contribution to the binding energy may be estimated to be a tiny 0.001 MeV.

VII. CONCLUSIONS

In the framework of chiral perturbation theory, three-nucleon forces begin at $\mathcal{O}(q^3)$, with a long range component which is due to the exchanges of two pions and relatively simple. At $\mathcal{O}(q^4)$, on the other hand, a large number of different processes intervene and a full

description becomes rather complex. For this reason, here we concentrate on a subset of $\mathcal{O}(q^4)$ interactions, namely that which still involves the exchanges of just two pions. This part of the 3NP is closely related with the πN amplitude, and the expansion of the former up to $\mathcal{O}(q^4)$ depends on the latter at $\mathcal{O}(q^3)$.

Our expressions for the potential are given in Eqs. (44-56) and the new chiral layer of the TPE-3NP considered in this work gives rise to both numerical corrections to strength coefficients of already existing terms (C_1^+, C_2^+, C_1^-) and new structures in the profile functions. Changes in numerical coefficients lay in the neighborhood of 10% and can be read in Tables II and III. New structures, on the other hand, arise either from loop functions representing form factors or the non-local terms associated with gradients acting on the wave function. They correspond to the terms proportional to the parameters C_3^+, C_2^- and C_3^- , which are small and compatible with perturbative effects.

In order to insert our results into a broader picture, in Table V we show the orders at which the various effects begin to appear, including the drift potential derived recently [40].

TABLE V: Chiral picture for two- and three-body forces.

beginning	TWO-BODY	TWO-BODY	THREE-BODY
$\mathcal{O}(q^0)$	OPEP: V_T^-, V_{SS}^-		
$\mathcal{O}(q^2)$	OPEP: V_D^-	TPEP: V_C^-, V_T^+, V_{SS}^+	
$\mathcal{O}(q^3)$		TPEP: $V_{LS}^-, V_T^-, V_{SS}^-, V_C^+, V_{LS}^+$	TPEP: C_1^-, C_1^+, C_2^+
$\mathcal{O}(q^4)$		TPEP: V_D^-, V_Q^+, V_D^+	TPEP: C_2^-, C_3^-, C_3^+

The influence of the new TPE-3NP over three-body observables has been assessed in both static and scattering environments, adopting the Argonne V_{18} potential for the two-body interaction. In order to reproduce the empirical triton binding energy, the $\mathcal{O}(q^4)$ potential requires a cutoff mass of 660 MeV. Comparing this with the value of 680 MeV for the 1983 Brazil TPE-3NP, one learns that the later version is more attractive.

In the study of proton-deuteron elastic scattering, we have calculated cross sections $\sigma(\theta)$, vector analyzing powers $A_y(\theta)$ of the proton and $iT_{11}(\theta)$ of the deuteron, and tensor analyzing powers $T_{20}(\theta)$, $T_{21}(\theta)$, and $T_{22}(\theta)$ of the deuteron, at energies of 3 and 28 MeV. Results are displayed in Figs. 6 and 7, where it is possible to see that there is little sensitivity to the changes induced in the strength parameters when one goes from $\mathcal{O}(q^3)$ to $\mathcal{O}(q^4)$. Old

problems, as the $A_y(\theta)$ puzzle, remain unsolved.

The present version of the TPE-3NP contains new structures, associated with loop integrals and non-local operators. Their influence over observables has been estimated and found to be at least one order of magnitude smaller than other three-body effects. A more detailed study of this part of the force is being carried on.

APPENDIX A: KINEMATICS

The coordinate describing the position of nucleon i is \mathbf{r}_i and one uses the combinations

$$\mathbf{R} = (\mathbf{r}_1 + \mathbf{r}_2 + \mathbf{r}_3)/3, \quad \mathbf{r} = \mathbf{r}_2 - \mathbf{r}_1, \quad \boldsymbol{\rho} = (2\mathbf{r}_3 - \mathbf{r}_1 - \mathbf{r}_2)/\sqrt{3}, \quad (\text{A1})$$

which yield

$$\mathbf{r}_1 = \mathbf{R} - \frac{\mathbf{r}}{2} - \frac{\boldsymbol{\rho}}{2\sqrt{3}}, \quad \mathbf{r}_2 = \mathbf{R} + \frac{\mathbf{r}}{2} - \frac{\boldsymbol{\rho}}{2\sqrt{3}}, \quad \mathbf{r}_3 = \mathbf{R} + \frac{\boldsymbol{\rho}}{\sqrt{3}}. \quad (\text{A2})$$

The momentum of nucleon i is \mathbf{p}_i and one defines

$$\mathbf{P} = \mathbf{p}_1 + \mathbf{p}_2 + \mathbf{p}_3, \quad \mathbf{p}_r = (\mathbf{p}_2 - \mathbf{p}_1)/2, \quad \mathbf{p}_\rho = (2\mathbf{p}_3 - \mathbf{p}_1 - \mathbf{p}_2)/2\sqrt{3}. \quad (\text{A3})$$

Initial momenta \mathbf{p} and final momenta \mathbf{p}' are used in the combinations

$$\mathbf{Q} = (\mathbf{P}' + \mathbf{P})/2, \quad \mathbf{q} = (\mathbf{P}' - \mathbf{P}), \quad (\text{A4})$$

$$\mathbf{Q}_r = (\mathbf{p}'_r + \mathbf{p}_r)/2, \quad \mathbf{q}_r = (\mathbf{p}'_r - \mathbf{p}_r), \quad (\text{A5})$$

$$\mathbf{Q}_\rho = (\mathbf{p}'_\rho + \mathbf{p}_\rho)/2, \quad \mathbf{q}_\rho = (\mathbf{p}'_\rho - \mathbf{p}_\rho). \quad (\text{A6})$$

In the CM, one has $\mathbf{P} = 0$ and the three-momenta are given by

$$\mathbf{p}_1 = -(\mathbf{Q}_r - \mathbf{q}_r/2) - (\mathbf{Q}_\rho - \mathbf{q}_\rho/2)/\sqrt{3}, \quad \mathbf{p}'_1 = -(\mathbf{Q}_r + \mathbf{q}_r/2) - (\mathbf{Q}_\rho + \mathbf{q}_\rho/2)/\sqrt{3}, \quad (\text{A7})$$

$$\mathbf{p}_2 = (\mathbf{Q}_r - \mathbf{q}_r/2) - (\mathbf{Q}_\rho - \mathbf{q}_\rho/2)/\sqrt{3}, \quad \mathbf{p}'_2 = (\mathbf{Q}_r + \mathbf{q}_r/2) - (\mathbf{Q}_\rho + \mathbf{q}_\rho/2)/\sqrt{3}, \quad (\text{A8})$$

$$\mathbf{p}_3 = 2(\mathbf{Q}_\rho - \mathbf{q}_\rho/2)/\sqrt{3}, \quad \mathbf{p}'_3 = 2(\mathbf{Q}_\rho + \mathbf{q}_\rho/2)/\sqrt{3}. \quad (\text{A9})$$

Energy conservation for on-shell particles yield the non-relativistic constraint

$$\mathbf{Q}_r \cdot \mathbf{q}_r + \mathbf{Q}_\rho \cdot \mathbf{q}_\rho = 0. \quad (\text{A10})$$

The momenta of the exchanged pions are written as

$$k = p_1 - p'_1, \quad k' = p'_2 - p_2, \quad (\text{A11})$$

$$k^0 = -(\mathbf{q}_r + \mathbf{q}_\rho/\sqrt{3}) \cdot (\mathbf{Q}_r + \mathbf{Q}_\rho/\sqrt{3})/m, \quad \mathbf{k} = \mathbf{q}_r + \mathbf{q}_\rho/\sqrt{3}, \quad (\text{A12})$$

$$k'^0 = (\mathbf{q}_r - \mathbf{q}_\rho/\sqrt{3}) \cdot (\mathbf{Q}_r - \mathbf{Q}_\rho/\sqrt{3})/m, \quad \mathbf{k}' = \mathbf{q}_r - \mathbf{q}_\rho/\sqrt{3}, \quad (\text{A13})$$

and the Mandelstam variables for nucleon 3 read

$$s = (p_3 + k)^2 = m^2 - (\mathbf{q}_r + \mathbf{q}_\rho/\sqrt{3}) \cdot (\mathbf{q}_r + 2\mathbf{Q}_r - \mathbf{q}_\rho/\sqrt{3} + 2\sqrt{3}\mathbf{Q}_\rho) + \mathcal{O}(q^4), \quad (\text{A14})$$

$$u = (p_3 - k')^2 = m^2 - (\mathbf{q}_r - \mathbf{q}_\rho/\sqrt{3}) \cdot (\mathbf{q}_r + 2\mathbf{Q}_r + \mathbf{q}_\rho/\sqrt{3} - 2\sqrt{3}\mathbf{Q}_\rho) + \mathcal{O}(q^4), \quad (\text{A15})$$

$$\nu = (s - u)/4m = -2\mathbf{q}_r \cdot \mathbf{Q}_\rho/\sqrt{3} + \mathcal{O}(q^4). \quad (\text{A16})$$

In the evaluation of the intermediate πN amplitude, one needs

$$[\bar{u}(\mathbf{p}') u(\mathbf{p})]^{(3)} \simeq 2m + \mathcal{O}(q^2), \quad (\text{A17})$$

$$\left[\frac{i}{2m} \bar{u}(\mathbf{p}') \sigma_{\mu\nu} (p' - p)^\mu K^\nu u(\mathbf{p}) \right]^{(3)} \simeq 2i \boldsymbol{\sigma}^{(3)} \cdot \mathbf{q}_\rho \times \mathbf{q}_r/\sqrt{3} + \mathcal{O}(q^4). \quad (\text{A18})$$

The πN vertex for nucleon 1 is associated with

$$[\bar{u}(\mathbf{p}') \gamma_5 u(\mathbf{p})]^{(1)} \simeq \boldsymbol{\sigma}^{(1)} \cdot (\mathbf{q}_r + \mathbf{q}_\rho/\sqrt{3}) + \mathcal{O}(q^3), \quad (\text{A19})$$

and results for nucleon 2 are obtained by making $\mathbf{q}_r \rightarrow -\mathbf{q}_r$.

APPENDIX B: SUBTHRESHOLD COEFFICIENTS

The polynomial parts of the amplitudes T_R^\pm , Eqs. (30-35), are determined by the sub-threshold coefficients of Ref. [15]. The terms relevant to the $\mathcal{O}(q^3)$ expansion are written as

[6]

$$d_{00}^+ = -\frac{2(2c_1 - c_3)\mu^2}{f_\pi^2} + \frac{8g_A^4\mu^3}{64\pi f_\pi^4} + \left[\frac{3g_A^2\mu^3}{64\pi f_\pi^4} \right]_{mr}, \quad (\text{B1})$$

$$d_{01}^+ = -\frac{c_3}{f_\pi^2} - \frac{48g_A^4\mu}{768\pi f_\pi^4} - \left[\frac{77g_A^2\mu}{768\pi f_\pi^4} \right]_{mr}, \quad (\text{B2})$$

$$d_{02}^+ = \left[\frac{193g_A^2}{15360\pi f_\pi^4\mu} \right]_{mr}, \quad (\text{B3})$$

$$d_{00}^- = \left[\frac{1}{2f_\pi^2} \right]_{WT} + \mathcal{O}(q^2), \quad (\text{B4})$$

$$b_{00}^- = \left[\frac{1}{2f_\pi^2} \right]_{WT} + \frac{2c_4m}{f_\pi^2} - \frac{g_A^4m\mu}{8\pi f_\pi^4} - \left[\frac{g_A^2m\mu}{8\pi f_\pi^4} \right]_{mr}, \quad (\text{B5})$$

$$b_{01}^- = \left[\frac{g_A^2m}{96\pi f_\pi^4\mu} \right]_{mr}, \quad (\text{B6})$$

where the parameters c_i and \tilde{d}_i are the usual coupling constants of the chiral lagrangians of order 2 and 3 respectively [41] and the *tilde* over the latter indicates that they were renormalized [15]. Terms within square brackets labeled (*mr*) in these results are due to the medium range diagrams shown in Fig. 3 and have been included explicitly into the functions D_{mr}^\pm and B_{mr}^\pm . Terms bearing the (*WT*) label were also explicitly considered in Eqs. (15-19). The subthreshold coefficients are determined from πN scatterig data and a set of experimental values is given in Ref. [13].

APPENDIX C: FUNCTIONS I^n

The functions I^n , describing loop contributions, are given by

$$I^n(\mathbf{r}_{31}, \mathbf{r}_{23}) = -\frac{16\pi}{\mu^2} \int \frac{d\mathbf{k}}{(2\pi)^3} \frac{d\mathbf{k}'}{(2\pi)^3} e^{i(\mathbf{k}\cdot\mathbf{r}_{31} + \mathbf{k}'\cdot\mathbf{r}_{23})} \left[\frac{t}{\mu^2} \right]^n \frac{1}{\mathbf{k}^2 + \mu^2} \frac{1}{\mathbf{k}'^2 + \mu^2} \Pi_t(t). \quad (\text{C1})$$

Using the definition Eq. (33) and the Jacobi variables Eq. (A1), one writes

$$I^n(\mathbf{r}_{31}, \mathbf{r}_{23}) = \left[\frac{4\nabla_\rho^2}{3\mu^2} \right]^n I(\mathbf{r}_{31}, \mathbf{r}_{23}), \quad (\text{C2})$$

$$I(\mathbf{r}_{31}, \mathbf{r}_{23}) = 128\pi \int_0^1 da \tan^{-1} \left[\frac{ma\sqrt{1-a^2}}{\mu(1-a^2/2)} \right] L(a; \mathbf{r}, \boldsymbol{\rho}) \quad (\text{C3})$$

$$L(a; \mathbf{r}, \boldsymbol{\rho}) = \int \frac{d\mathbf{q}}{(2\pi)^3} \frac{d\mathbf{Q}}{(2\pi)^3} \frac{e^{i(\mathbf{Q}\cdot\mathbf{r} - \sqrt{3}\mathbf{q}\cdot\boldsymbol{\rho}/2)}}{a^2\mathbf{q}^2 + 4\mu^2} \frac{1}{[(\mathbf{Q}-\mathbf{q})^2 + \mu^2]} \frac{1}{[(\mathbf{Q}+\mathbf{q})^2 + \mu^2]}. \quad (\text{C4})$$

The numerical evaluation of the function L is can be simplified by using alternative representations.

- **form 1:** One uses the Feynman procedure for manipulating denominators, which yields

$$\begin{aligned}
L(a; \mathbf{r}, \boldsymbol{\rho}) &= \int_0^1 db \int \frac{d\mathbf{q}}{(2\pi)^3} \frac{d\mathbf{Q}}{(2\pi)^3} \frac{e^{i(\mathbf{Q} \cdot \mathbf{r} - \sqrt{3} \mathbf{q} \cdot \boldsymbol{\rho}/2)}}{a^2 \mathbf{q}^2 + 4\mu^2} \frac{1}{[(\mathbf{Q}^2 + \mathbf{q}^2/4 + \mu^2) - (1-2b)\mathbf{q} \cdot \mathbf{Q}]^2} \\
&= \frac{1}{8\pi} \int_0^1 db \int \frac{d\mathbf{q}}{(2\pi)^3} \frac{e^{i[(1-2b)\mathbf{r} - \sqrt{3}\boldsymbol{\rho}] \cdot \mathbf{q}/2}}{a^2 \mathbf{q}^2 + 4\mu^2} \frac{e^{-\Theta r}}{\Theta}, \\
\Theta &= \sqrt{\mu^2 + b(1-b)\mathbf{q}^2}.
\end{aligned} \tag{C5}$$

Performing the angular integration over \mathbf{q} , one has

$$L(a; \mathbf{r}, \boldsymbol{\rho}) = \frac{1}{16\pi^3} \int_0^1 db \int dq q \frac{e^{-\Theta r}}{\Theta(a^2 \mathbf{q}^2 + 4\mu^2)} \frac{\sin q [(1-2b)\mathbf{r} - \sqrt{3}\boldsymbol{\rho}]/2}{[(1-2b)\mathbf{r} - \sqrt{3}\boldsymbol{\rho}]/2}. \tag{C6}$$

- **form 2:** The Fourier transform

$$\frac{1}{\mathbf{k}^2 + \mu^2} = \int d\mathbf{x} e^{-i\mathbf{k} \cdot \mathbf{x}} \frac{e^{-\mu x}}{4\pi x} \tag{C7}$$

allows one to write

$$L(a; \mathbf{r}, \boldsymbol{\rho}) = \frac{1}{64\pi^3} \frac{1}{a^2} \int dz \frac{e^{-\mu|\mathbf{r}_{31} + \mathbf{z}|}}{|\mathbf{r}_{31} + \mathbf{z}|} \frac{e^{-\mu|\mathbf{r}_{23} - \mathbf{z}|}}{|\mathbf{r}_{23} - \mathbf{z}|} \frac{e^{-2\mu z/a}}{z}. \tag{C8}$$

These results may be further simplified by means of approximations.

- **heavy baryon approximation:** In the limit $m \rightarrow \infty$, corresponding to the heavy baryon case, one uses $F(a) \rightarrow 4\pi/a^2$ in Eq. (33) and Eqs. (C5) and (C7) yield, respectively,

$$I(\mathbf{r}_{31}, \mathbf{r}_{23}) \simeq \frac{2}{\pi} \int_0^1 db \int_0^\infty dq \left[\tan^{-1} \frac{q}{2\mu} \right] \frac{e^{-\Theta r}}{\mu \Theta} \frac{\sin q [(1-2b)\mathbf{r} - \sqrt{3}\boldsymbol{\rho}]/2}{[(1-2b)\mathbf{r} - \sqrt{3}\boldsymbol{\rho}]/2}, \tag{C9}$$

$$I(\mathbf{r}_{31}, \mathbf{r}_{23}) \simeq \frac{1}{\pi} \int dz \frac{e^{-\mu|\mathbf{r}_{31} + \mathbf{z}|}}{|\mathbf{r}_{31} + \mathbf{z}|} \frac{e^{-\mu|\mathbf{r}_{23} - \mathbf{z}|}}{|\mathbf{r}_{23} - \mathbf{z}|} \frac{e^{-2\mu z}}{2\mu z^2}. \tag{C10}$$

- **multipole approximation:** The integrand in Eq. (C10) is peaked around $z = 0$ and a multipole expansion of the Yukawa functions produces

$$I(\mathbf{r}_{31}, \mathbf{r}_{23}) \simeq U(x_{31}) U(x_{23}) + \dots. \tag{C11}$$

The same result can also be obtained by using the expansion $\Pi_t(t) \sim -\pi[1 + t/12\mu^2 + t^2/80\mu^4 + \dots]$, valid for low t , directly into Eq. (C1).

APPENDIX D: NON-LOCAL TERM

In configuration space, the variable \mathbf{Q}_ρ corresponds to a non-local operator, represented by a gradient acting on the wave function. In order to make the dependence of \bar{t}_3 on \mathbf{Q}_ρ explicit, one writes

$$\bar{t}_3 = [Q_\rho]_i X_i(\mathbf{q}_r, \mathbf{q}_\rho), \quad (\text{D1})$$

where \mathbf{X} is a generic three-vector, and evaluates the matrix element

$$\begin{aligned} \langle \psi | W | \psi \rangle &= - \left[\frac{1}{(2\pi)} \right]^{12} \int d\mathbf{r}' d\boldsymbol{\rho}' d\mathbf{r} d\boldsymbol{\rho} \psi^*(\mathbf{r}', \boldsymbol{\rho}') \psi(\mathbf{r}, \boldsymbol{\rho}) \int d\mathbf{Q}_r d\mathbf{Q}_\rho d\mathbf{q}_r d\mathbf{q}_\rho \\ &\times e^{i[\mathbf{Q}_r \cdot (\mathbf{r}' - \mathbf{r}) + \mathbf{Q}_\rho \cdot (\boldsymbol{\rho}' - \boldsymbol{\rho}) + \mathbf{q}_r \cdot (\mathbf{r}' + \mathbf{r})/2 + \mathbf{q}_\rho \cdot (\boldsymbol{\rho}' + \boldsymbol{\rho})/2]} \bar{t}_3(\mathbf{Q}_r, \mathbf{Q}_\rho, \mathbf{q}_r, \mathbf{q}_\rho) \\ &= - \left[\frac{1}{(2\pi)} \right]^6 \int d\mathbf{r} d\boldsymbol{\rho} \left\{ \left[\frac{i}{2} \nabla_\rho \psi^*(\mathbf{r}, \boldsymbol{\rho}) \right]_i \psi(\mathbf{r}, \boldsymbol{\rho}) + \psi^*(\mathbf{r}, \boldsymbol{\rho}) \left[-\frac{i}{2} \nabla_\rho \psi(\mathbf{r}, \boldsymbol{\rho}) \right]_i \right\} \\ &\times \int d\mathbf{q}_r d\mathbf{q}_\rho e^{i[\mathbf{q}_r \cdot \mathbf{r} + \mathbf{q}_\rho \cdot \boldsymbol{\rho}]} X_i(\mathbf{q}_r, \mathbf{q}_\rho). \end{aligned} \quad (\text{D2})$$

This yields the potential

$$V_3(\mathbf{r}, \boldsymbol{\rho}) = - \frac{[2/\sqrt{3}]^3}{(2\pi)^6} \left[-\frac{i}{2} \overleftrightarrow{\nabla}_\rho \right]_i \int d\mathbf{q}_r d\mathbf{q}_\rho e^{i[\mathbf{q}_r \cdot \mathbf{r} + \mathbf{q}_\rho \cdot \boldsymbol{\rho}]} X_i(\mathbf{q}_r, \mathbf{q}_\rho), \quad (\text{D3})$$

where the operator $\overleftrightarrow{\nabla} = \overrightarrow{\nabla} - \overleftarrow{\nabla}$ acts *only* on the wave function. An alternative form can be obtained by integrating Eq. (D2) by parts, and one finds

$$\begin{aligned} V_3(\mathbf{r}, \boldsymbol{\rho}) &= - \frac{[2/\sqrt{3}]^3}{(2\pi)^6} \left\{ \left[\int d\mathbf{q}_r d\mathbf{q}_\rho e^{i[\mathbf{q}_r \cdot \mathbf{r} + \mathbf{q}_\rho \cdot \boldsymbol{\rho}]} \mathbf{X}(\mathbf{q}_r, \mathbf{q}_\rho) \right] \cdot [-i \nabla_\rho^{wf}] \right. \\ &\quad \left. - \left[\frac{i}{2} \nabla_\rho \cdot \int d\mathbf{q}_r d\mathbf{q}_\rho e^{i[\mathbf{q}_r \cdot \mathbf{r} + \mathbf{q}_\rho \cdot \boldsymbol{\rho}]} \mathbf{X}(\mathbf{q}_r, \mathbf{q}_\rho) \right] \right\}. \end{aligned} \quad (\text{D4})$$

In the case of the three-body force, the only non-local contribution is associated with the subamplitude D^- , Eq. (37), which yields

$$X_i = -i \boldsymbol{\tau}^{(1)} \times \boldsymbol{\tau}^{(2)} \cdot \boldsymbol{\tau}^{(3)} \frac{1}{\mathbf{k}^2 + \mu^2} \frac{1}{\mathbf{k}'^2 + \mu^2} \boldsymbol{\sigma}^{(1)} \cdot \mathbf{k} \boldsymbol{\sigma}^{(2)} \cdot \mathbf{k}' \left[\frac{g_A^2 (g_A^2 - 1)}{\sqrt{3} 8f_\pi^4 m} \right] (\mathbf{k}' + \mathbf{k})_i. \quad (\text{D5})$$

The action of ∇_ρ on the second term of Eq. (D4) gives rise to an integrand proportional to $(\mathbf{k}'^2 - \mathbf{k}^2)$, which has short range and does not contribute to the TPE-3NP. Therefore it is neglected.

[1] M. Taketani, S. Nakamura, and T. Sasaki, Prog. Theor. Phys. **6**, 581 (1951).

- [2] S. Weinberg, Phys. Lett. B **251**, 288 (1990); Nucl. Phys. B **363**, 3 (1991).
- [3] S. Weinberg, Phys. Lett. B **295**, 114 (1992).
- [4] C. Ordóñez and U. van Kolck, Phys. Lett. B **291**, 459 (1992); C. Ordóñez, L. Ray, and U. van Kolck, Phys. Rev. Lett. **72**, 1982 (1994); Phys. Rev. C **53**, 2086 (1996).
- [5] N. Kaiser, R. Brockman, and W. Weise, Nucl. Phys. **A625**, 758 (1997); N. Kaiser, Phys. Rev. C **64**, 057001 (2001); Phys. Rev. C **65**, 017001 (2001); E. Epelbaum, W. Glöckle, and U-G. Meissner, Nucl. Phys. **A637**, 107 (1998); *ibid.* **A671**, 295 (2000); D. R. Entem and R. Machleidt, Phys. Rev. C **66**, 014002 (2002).
- [6] R. Higa and M. R. Robilotta, Phys. Rev. C **68**, 024004 (2003).
- [7] R. Higa, M. R. Robilotta, and C. A. da Rocha, Phys. Rev. C **69**, 034009 (2004).
- [8] S. A. Coon, M. D. Scadron, P. C. McNamee, B. R. Barrett, D. W. E. Blatt, and B. H. J. McKellar, Nucl. Phys. **A317**, 242 (1979).
- [9] S. A. Coon and W. Glöckle, Phys. Rev. C **23**, 1790 (1981).
- [10] H. T. Coelho, T. K. Das, and M. R. Robilotta, Phys. Rev. C **28**, 1812 (1983).
- [11] J. L. Friar, Phys. Rev. C **60**, 034002 (1999).
- [12] S-N. Yang, Phys. Rev. C **10**, 2067 (1974).
- [13] G. Höhler, group I, vol.9, subvol.b, part 2 of Landölt-Bornstein Numerical data and Functional Relationships in Science and Technology, ed. H.Schopper, 1983; G. Höhler, H. P. Jacob, and R. Strauss, Nucl. Phys. **B39**, 273 (1972).
- [14] T. Becher and H. Leutwyler, Eur. Phys. Journal C **9**, 643 (1999).
- [15] T. Becher and H. Leutwyler, JHEP **106**, 17 (2001).
- [16] J. C. Ward, Phys. Rev. **78**, 1824 (1950); Y. Takahashi, Nuovo Cimento **6**, 370 (1957); L. S. Brown, W. J. Pardee, and R. Peccei, Phys. Rev. D **4**, 2801 (1971).
- [17] M. Mojžiš and J. Kambor, Phys. Lett. B **476**, 344 (2000).
- [18] J. Gasser, M. E. Sainio, and A. Švarc, Nucl. Phys. **B307**, 779 (1988).
- [19] G. Höhler, H. P. Jacob, and R. Strauss, Nucl. Phys. **B39**, 273 (1972).
- [20] S. Weinberg, Phys. Rev. Lett. **17**, 616 (1966).
- [21] Y. Tomozawa, Nuovo Cimento A **46**, 707 (1966).
- [22] M. R. Robilotta, Phys. Rev. C **63**, 044004 (2001).
- [23] I. P. Cavalcante, M. R. Robilotta, J. Sá Borges, D. de O. Santos, and G. R. S. Zarnauskas, Phys. Rev. C **72**, 065207 (2005).

- [24] J. L. Friar, D. Huber, and U. van Kolck, Phys. Rev. C **59**, 53 (199); U. van Kolck, Ph. D. thesis, University of Texas, 1993; C. Ordóñez and U. van Kolck, Phys. Lett. B **291**, 459 (1992); U. van Kolck, Phys. Rev. C **49**, 2932 (1994).
- [25] J. Gasser, H. Leutwyler, and M. E. Sainio, Phys. Lett. B **253**, 252, 260 (1991).
- [26] P. Büttiker and U.-G. Meissner, Nucl. Phys. **A668**, 97 (2000).
- [27] N. Fettes and U.-G. Meissner, Nucl. Phys. **A693**, 693 (2001).
- [28] S. A. Coon and H. K. Han, Few-Body Syst. **30**, 131 (2001).
- [29] M. R. Robilotta and H. T. Coelho, Nucl. Phys. **A460**, 645 (1986).
- [30] M. G. Olsson and E. T. Osypowski, Nucl. Phys. **B101**, 136 (1975); E. T. Osypowski, Nucl. Phys. **B21**, 615 (1970).
- [31] T. Sasakawa and S. Ishikawa, Few-Body Syst. **1**, 3 (1986).
- [32] S. Ishikawa, Few-Body Syst. **32**, 229 (2003).
- [33] S. Ishikawa, Few-Body Syst. (to be published), nucl-th/0701044.
- [34] R. B. Wiringa, V. G. J. Stoks, and R. Schiavilla, Phys. Rev. C **51**, 38 (1995).
- [35] K. Sagara, H. Oguri, S. Shimizu, K. Maeda, H. Nakamura, T. Nakashima, and S. Morinobu, Phys. Rev. C **50**, 576 (1994).
- [36] S. Shimizu, K. Sagara, H. Nakamura, K. Maeda, T. Miwa, N. Nishimori, S. Ueno, T. Nakashima, and S. Morinobu, Phys. Rev. C **52**, 1193 (1995).
- [37] S. Ishikawa, M. Tanifuji, and Y. Iseri, Phys. Rev. C **67**, 061001(R) (2003).
- [38] S. Ishikawa, M. Tanifuji, and Y. Iseri, in *Proc. of the Seventeenth International IUPAP Conference on Few-Body Problems in Physics, Durham, North Carolina, USA, 2003*, edited by W. Glöckle and W. Tornow, (Elsevier, Amsterdam, 2004) S61.
- [39] K. Hatanaka, N. Matsuoka, H. Sakai, T. Saito, K. Hosono, Y. Koike, M. Kondo, K. Imai, H. Shimizu, T. Ichihara, K. Nisimura, and A. Okihana, Nucl. Phys. **A426**, 77 (1984).
- [40] M. R. Robilotta, Phys. Rev. C **74**, 044002 (2006).
- [41] V. Bernard, N. Kaiser, J. Kambor, and U.-G. Meissner, Nucl. Phys. **B388**, 315 (1992).